Transport Mechanism of Enhanced Performance in an Amorphous/Monoclinic Mixed-Phase Ga_2O_3 Solar-Blind Deep Ultraviolet Photodetector

Haowen Liu[#], Honglin Li[#], Shuren Zhou, Hong Zhang, Shiqiang Fan, Yuting Cui, Chunyang Kong, Lijuan Ye*, Yuanqiang Xiong* and Wanjun Li*

Chongqing Key Laboratory of Photo-Electric Functional Materials, College of Physics and Electronic Engineering, Chongqing Normal University, Chongqing, 401331, People's Republic of China

[#] H. Liu and H. Li contributed equally to this work.

Correspondence: E-mail: liwj@cqnu.edu.cn (W.J. Li); E-mail: ylj2592924@163.com (L. Ye); E-mail: xyq.0810@163.com (Y.Q. Xiong). Tel.: +86 23 65362779.

#1 Supplementary Figures

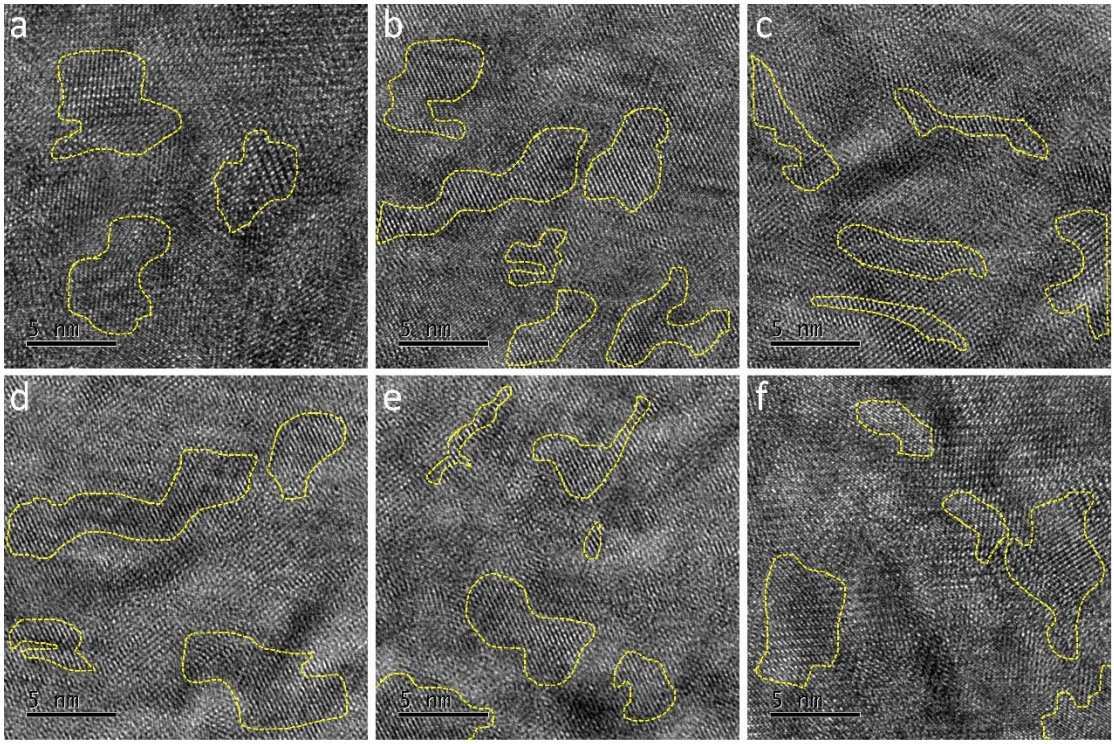

Figure S1. (**a**-**f**) HRTEM images of different regions of the S400. The yellow closed curve is crystalline phase Ga2O3. It is obvious that there are randomly distributed crystalline phases Ga2O3 in different regions, indicating that the amorphous and crystalline phases are continuously distributed in the prepared Ga2O3 film (S400).

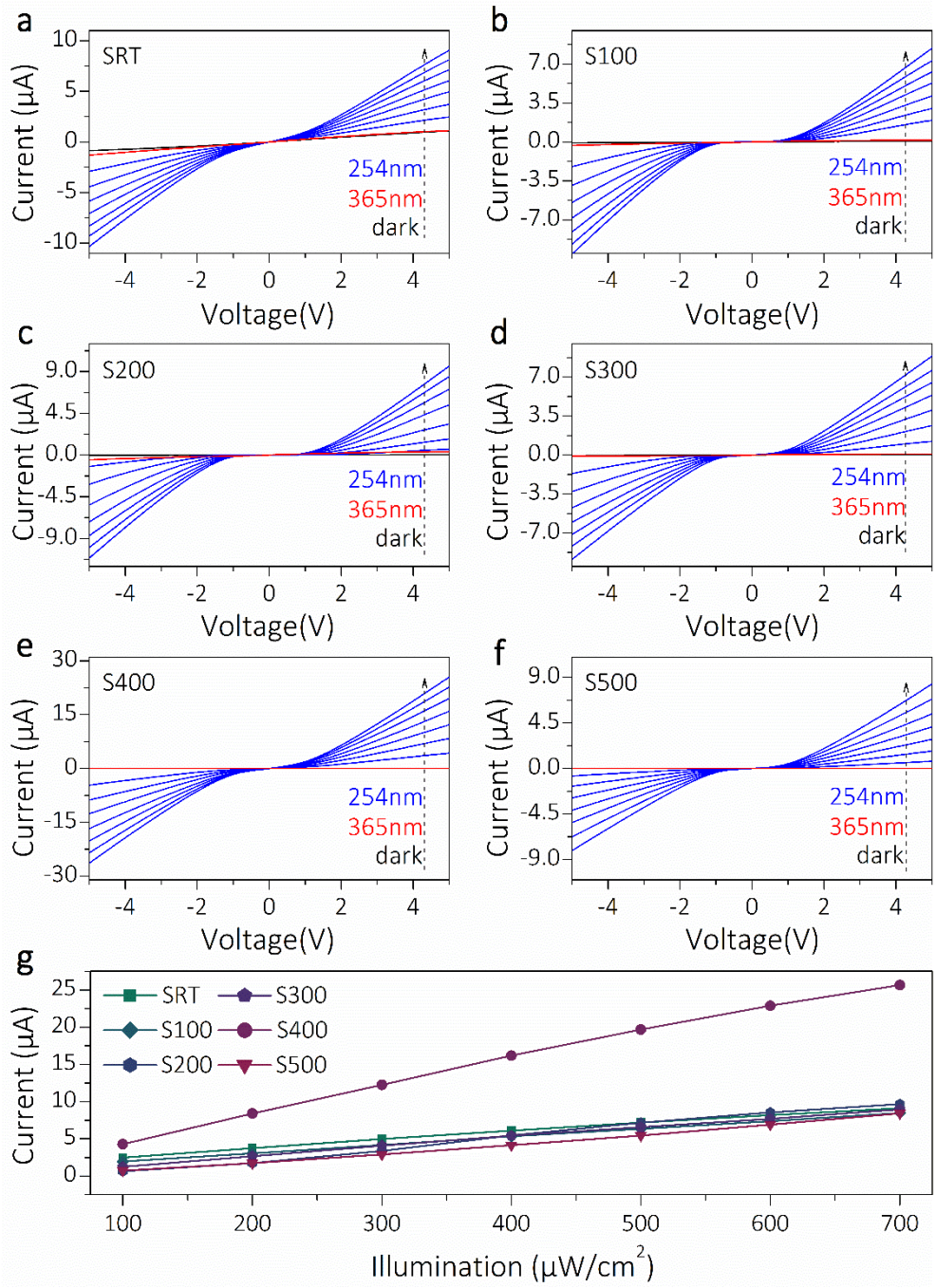

Figure S2. (**a**-**f**) The I-V characteristics curve of Ga2O3 film PDs (SRT-S500) under dark, 365 nm and 254 nm illumination (the light intensities of 254 nm are 100-700 μW/cm2, and the one of 365 nm is 500 μW/cm2). (g) The corresponding photocurrent of SRT-S500 as a function of light intensities.

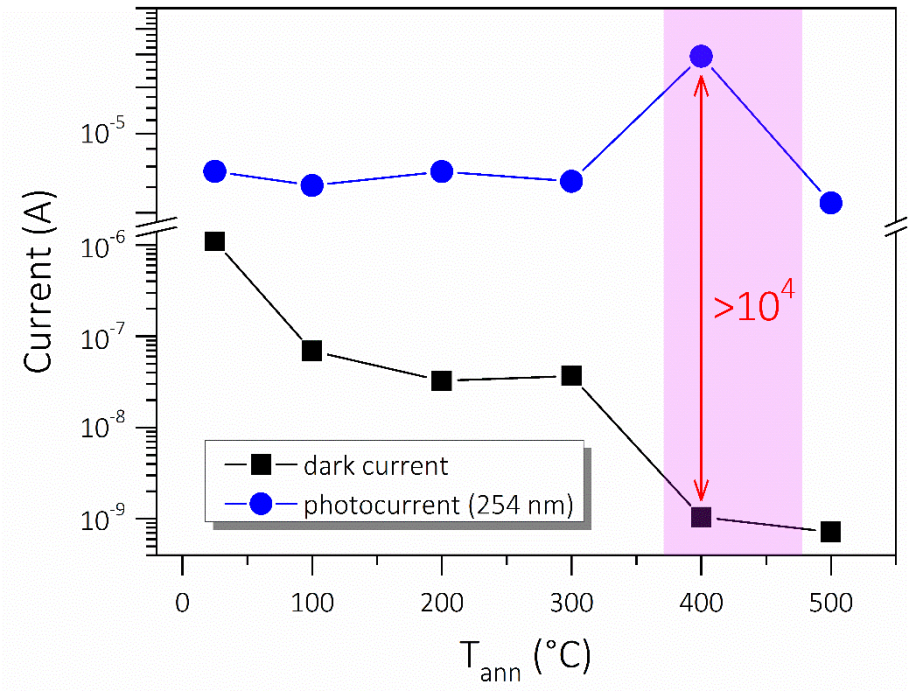

Figure S3. Dark current and photocurrent variation curves of Ga_2O_3 PDs. As the annealing temperature increases, the dark current of the PD decreases continuously, and the decrease of the mixed-phase Ga_2O_3 PD (S400) is more significant. The photocurrent remained basically constant except for the obvious enhancement of S400. The mixed-phase Ga_2O_3 PD (S400) exhibits the superior PDCR greater than 104.

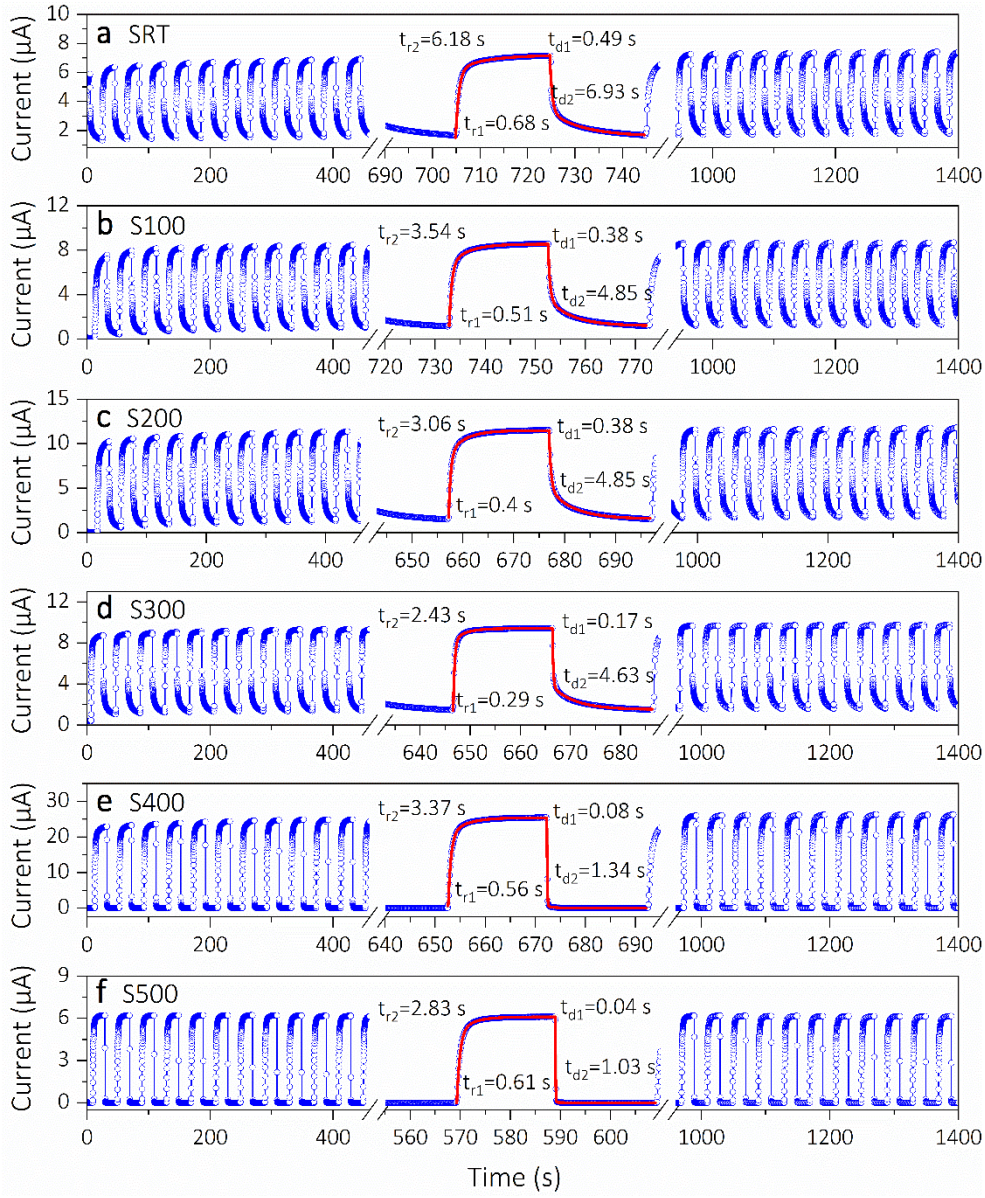

Figure S4. (**a**-**f**) Transient response of the PDs (SRT-S500) under the 254 nm light illumination with the power density of 500 μW/cm2 at 5 V. The dynamic response of all PDs presents good stability and reproducibility, and fitting results show that the decay time gradually increases with the degree of crystallization.

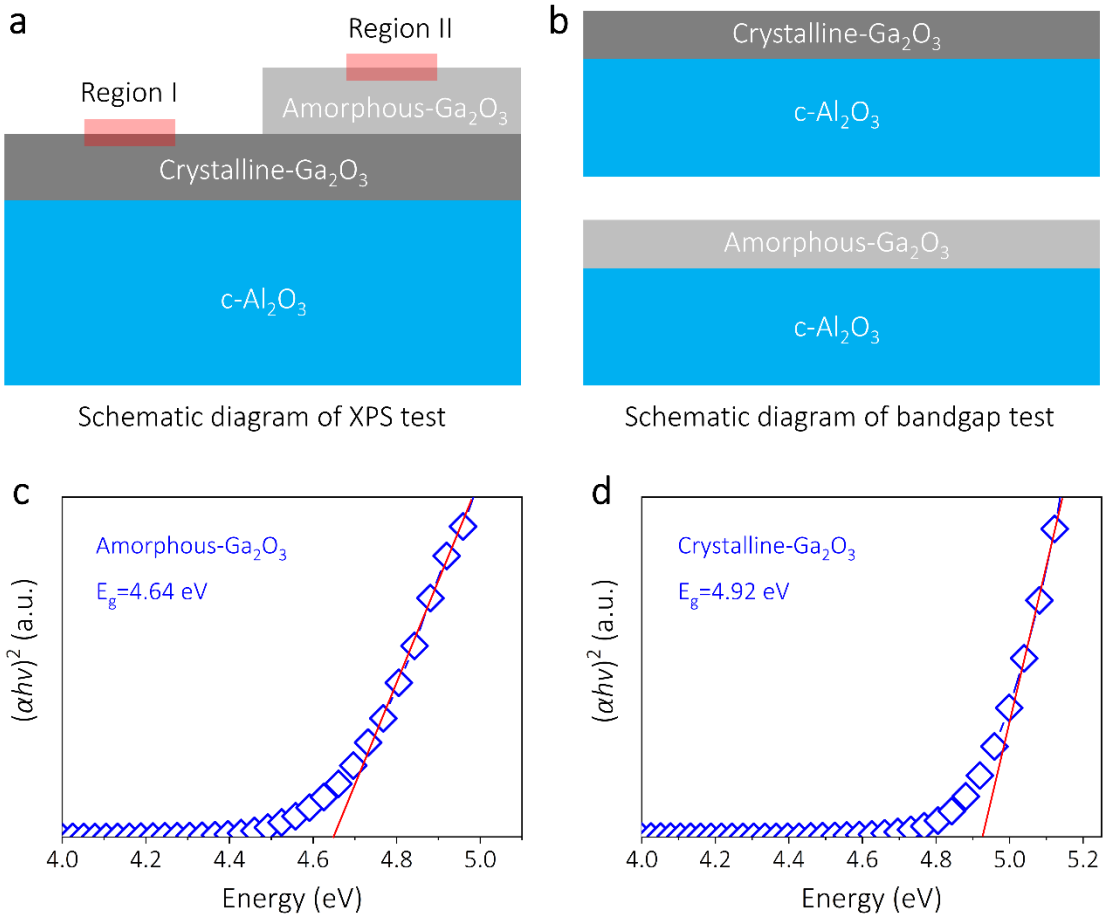

Figure S5. (**a**) The schematic diagram for XPS tests, a sample with fully covered crystalline layer and semi-covered amorphous layer is used for XPS test, and the data is obtained in the annotated regions. (**b**) The schematic diagram for absorption spectrum tests, two samples with fully covered amorphous and crystalline Ga_2O_3 films are used for absorption spectrum tests. The variation of $(ahv)^2$ with photon energy (hv) of (**c**) amorphous Ga_2O_3 and (**d**) crystalline Ga_2O_3. It shows that the E_g of amorphous and crystalline are 4.64 and 4.92 eV, respectively.

#2 Supplementary Notes

Note 1 Deposition of the Ga_2O_3 thin films

A series of amorphous Ga_2O_3 films were deposited on *c*-plane sapphire substrates by rf magnetron sputtering at room temperature. Before deposition, all the substrates were cleaned in deionized water, ethyl alcohol, acetone, ethyl alcohol, and deionized water for 10 min successively. A ceramic Ga_2O_3 (5N purity) disk (100 mm in diameter) was employed as the sputtering target, and substrate-target distance is about 10 cm. The base chamber pressure was evacuated to be below 5.0×10^{-4} Pa, and the Ar flow rate and work pressure were fixed at 40 SCCM and 2 Pa, respectively. Subsequently, part of the samples underwent isochronal annealing at 100, 200, 300, 400, and 500 °C in an argon atmosphere for 2 h, labeled as S100, S200, S300, S400, S500, respectively. The reference sample without post-annealing is named as SRT.

Note 2 Main performance index calculations

The responsivity (R), defined as the photocurrent generated perunit power of the incident light on the effective area of the PD, is given by the equation [1]:

$$R = \frac{I_{\text{photo}} - I_{\text{dark}}}{P_\lambda S} \tag{S1}$$

where, I_{dark} and I_{photo} denote dark current and photocurrent, respectively. P_λ is the light intensity of DUV light with 254 nm (500 μW/cm²), S is the effective irradiation area (0.03 cm²).

The detectivity (D^*), another key figure-of-merit of PD, which usually describes the smallest detectable signal including both the photoresponse and the noise floor, can be estimated by the relationship [2]:

$$D^* = \frac{RS^{\frac{1}{2}}}{(2qI_{\text{dark}})^{\frac{1}{2}}} \tag{S2}$$

where S is the effective irradiation area, R is the responsivity, q is the electronic charge, I_{dark} is the dark current.

External quantum efficiency (EQE) is defined as the number of electrons detected per incident photon and is given by [3]:

$$EQE = \frac{hc}{q\lambda}R \times 10^2\% \tag{S3}$$

where c is the light speed, λ is the wavelength of DUV light, h is the Planck's constant.

The photo-to-dark current ratio (PDCR) as the function of the 5 V bias voltages at various light intensities, and gives the information about signal-to-noise ratio of the PDs and can be determined by the relation [4]:

$$PDCR = \frac{I_{\text{photo}} - I_{\text{dark}}}{I_{\text{dark}}} \tag{S4}$$

where I_{photo} is the photocurrent at 254 nm light illumination, and I_{dark} is dark current given above.

The rejection ratio (R_{254}/R_{365}) is the ratio of the responsivity between 254 nm and 365 nm. High R_{254}/R_{365} demonstrates that the Ga_2O_3 PD is sensitive to the solar-blind radiation signal, undiscerning to the UVA (365 nm) light, and presenting a high spectral selectivity of the solar-blind region [5].

For a more detailed investigation, the transient response curves were fitted with a

biexponential relaxation equation as follows [6]:

$$I = I_0 + Ae^{-t/\tau_1} + Be^{-t/\tau_2} \quad \text{(S4)}$$

where I_0 is the steady-state photocurrent, t is the time, A and B are the constants, τ_1 and τ_2 are the relaxation time constants corresponding to two components (fast and slow). τ_r and τ_d denote the rise and decay time constants, respectively.

Note 3 Band alignment calculation

The valence band offset and conduction band offset can be calculated according to the following equations [7]:

$$\Delta E_V = \left(E_{Ga\ 2p3/2}^{\beta-Ga_2O_3} - E_{VBM}^{\beta-Ga_2O_3}\right) - \left(E_{Ga\ 2p3/2}^{a-Ga_2O_3} - E_{VBM}^{a-Ga_2O_3}\right) - \left(E_{Ga\ 2p3/2}^{\beta-Ga_2O_3} - E_{Ga\ 2p3/2}^{a-Ga_2O_3}\right) \quad \text{(S6)}$$

And

$$\Delta E_C = E_g^{\beta-Ga_2O_3} - E_g^{a-Ga_2O_3} - \Delta E_V \quad \text{(S7)}$$

where $\left(E_{Ga\ 2p3/2}^{\beta-Ga_2O_3} - E_{VBM}^{\beta-Ga_2O_3}\right)$ is the energy differences between core energy level and the valence band maximum (VBM) for crystalline Ga_2O_3, while $\left(E_{Ga\ 2p3/2}^{a-Ga_2O_3} - E_{VBM}^{a-Ga_2O_3}\right)$ is for the amorphous Ga_2O_3. $\left(E_{Ga\ 2p3/2}^{\beta-Ga_2O_3} - E_{Ga\ 2p3/2}^{a-Ga_2O_3}\right)$ is the difference between the crystalline and amorphous Ga_2O_3 core energy levels measured separately. $\left(E_g^{\beta-Ga_2O_3}\right)$ and $\left(E_g^{a-Ga_2O_3}\right)$ are the bandgaps of crystalline and amorphous Ga_2O_3, respectively. According to Eq. (S6), $\left(E_{Ga\ 2p3/2}^{\beta-Ga_2O_3} - E_{VBM}^{\beta-Ga_2O_3}\right)$ and $\left(E_{Ga\ 2p3/2}^{a-Ga_2O_3} - E_{VBM}^{a-Ga_2O_3}\right)$ could be calculated to be 1115.24 eV and 1115.03 eV, respectively. Based on these binding energy values, $\Delta E_V = 1117.30 - 2.06 - 1117.60 - (-2.57) - (-0.30) = 0.51$ eV and $\Delta E_C = 4.92 - 4.64 - (-0.51) = 0.80$ eV, Therefore, the band offsets in valence band ΔE_V and conduction band ΔE_C are calculated to be 0.51 eV and 0.80 eV, respectively.

#3 Supplementary References

1. Zheng, W.; Huang, F.; Zheng, R.; Wu, H. Low-Dimensional Structure Vacuum-Ultraviolet-Sensitive (λ< 200 nm) Photodetector with Fast-Response Speed Based on High-Quality AlN Micro/Nanowire. *Adv. Mater.* **2015**, *27*, 3921-3927, doi:10.1002/adma.201500268.
2. Zhao, B.; Wang, F.; Chen, H.Y.; Wang, Y.P.; Jiang, M.M.; Fang, X.S.; Zhao, D.X. Solar-Blind Avalanche Photodetector Based On Single ZnO-Ga_2O_3 Core-Shell Microwire. *Nano Lett.* **2015**, *15*, 3988-3993, doi:10.1021/acs.nanolett.5b00906.
3. Xu, J.J.; Zheng, W.; Huang, F. Gallium Oxide Solar-Blind Ultraviolet Photodetector: A Review. *J. Mater. Chem. C* **2019**, *7*, 8753-8770, doi:10.1039/c9tc02055a.
4. Li, S.; Guo, D.Y.; Li, P.G.; Wang, X.; Wang, Y.H.; Yan, Z.Y.; Liu, Z.; Zhi, Y.S.; Huang, Y.Q.; Wu, Z.P.; et al. Ultrasensitive, Superhigh Signal-to-Noise Ratio, Self-Powered Solar-Blind Photodetector Based on n-Ga_2O_3/p-CuSCN Core-Shell Microwire Heterojunction. *ACS Appl. Mater. Interfaces* **2019**, *11*, 35105-35114, doi:10.1021/acsami.9b11012.
5. Chen, X.H.; Ren, F.F.; Gu, S.L.; Ye, J.D. Review of gallium-oxide-based solar-blind

ultraviolet photodetectors. *Photonics Res.* **2019**, *7*, 381-415, doi:10.1364/prj.7.000381.

6. Arora, K.; Goel, N.; Kumar, M.; Kumar, M. Ultrahigh Performance of Self-Powered β-Ga_2O_3 Thin Film Solar-Blind Photodetector Grown on Cost-Effective Si Substrate Using High-Temperature Seed Layer. *ACS Photonics* **2018**, *5*, 2391-2401, doi:10.1021/acsphotonics.8b00174.
7. Kraut, E.A.; Grant, R.W.; Waldrop, J.R.; Kowalczyk, S.P. Precise Determination of the Valence-Band Edge in X-Ray Photoemission Spectra: Application to Measurement of Semiconductor Interface Potentials. *Phys. Rev. Lett.* **1980**, *44*, 1620-1623, doi:10.1103/PhysRevLett.44.1620.